Bioinspired nanovalves with selective permeability and pH sensitivity

Z. Zheng, X. Huang, M. Schenderlein, H. Moehwald, G.-K. Xu and D. G. Shchukin

(Supplementary information)

1. Material and Reagents

Tetraethyl orthosilicate (reagent grade, 98%), sodium hydroxide solution (~1.0 M NaOH), hexadecyltrimethylammonium bromide (≥98%), toluene (anhydrous, 99.8%), 1H-benzotriazole (≥98.0%), cobalt(II) nitrate hexahydrate (ACS reagent, ≥98%), copper(II) sulfate pentahydrate (ACS reagent, ≥98.0%) and sodium carbonate (> 99.95% dry basis) were all purchased from Sigma-Aldrich. (Trimethoxysilylpropyl)-ethylenediamine triacetic acid trisodium salt (45% in water) was bought from ABCR GmbH & CO. KG.

2. Synthetic procedure

MCM-41 nanoparticles: the silica mesorporous nanoparticles were fabricated according to the method reported[1]. Briefly, 950 mL of deionized water, 2 g of hexadecyltrimethylammonium bromide and 14 mL of sodium hydroxide solution (~1.0 M NaOH) were mixed and preheated at 80 ℃ for 1 h. Then 10 mL of TEOS was dropped in within 30 min. The mixture was further heated for 2 hours followed by cooling down at ambient conditions. The template was removed by calcination at 550 ℃.

Loading procedure: The subsequent loading of the containers with cargo molecules was conducted from corresponding solutions under reduced pressure (30 mbar) for three times consequently. To obtain loaded nanocontainers without surface absorbed BTA, a quick washing method was developed to prevent spontaneous leakage of the loaded active compounds to the maximum extent[2]. A home-made washing setup was simply composed of a piece of filter paper (0.05 μm pore diameter), a funnel and a pump. Before washing, a thin layer of pristine solid was carefully deposited on the filter paper. Then water was added on the solid droplet. The procedure was repeated

for several times till the released amount of BTA (determined by UV analysis) remained constant.

Coatings: The water-based organic coating is a two-component, model coating developed as a primer for aerospace applications by Mankiewicz GmbH. The resin component is an epoxy based primer, which consists of synthetic resins and water. The hardener component consists of polyamines in water. Water suspension of the BTA loaded containers was added to the pre-mixed two components under stirring. The amount of water used to re-disperse the containers prior to mixing with the paint was only 5 wt% of the paint and had no detrimental effect on the paint formulation. The dummy coating is the epoxy based primer containing 5 wt% of free, non-encapsulated BTA. The samples were deposited on the aluminum AA2024-T3 plates (scrubbed clean with NaOH, then nitric acid) using a spray technique and dried at 80 ° C for 1 h after a flash-off time of 15 min at room temperature.

3. Characterization

HADDF STEM image and STEM EDX mapping were recorded from Cs–corrected Titan 80–300 microscopes operated at 300 kV. Structure, size and porosity of the samples were characterized by TEM (Zeiss EM912), BET (Macromeritics TriStar 3000 system), DLS (Malvern Zetasizer 4), SEM (Hitachi S-4800). Thermogravimetric analysis (TGA) was performed on Netzsch TG 209 F1 at a scanning rate of 20 K/min under a nitrogen atmosphere. Aqueous suspensions containing 1 mL of precipitate and 4 mL of water were titrated against HCl standard solution with pH = 1 by using a Metrohm Autotitrator. Titration allowed for determination of approximate pH and exothermal ranges in which the precipitates react with acid.

SVET (Scanning Vibration Electrode Technique) measurements of the self-healing properties were performed on the substrate area of 3×3 mm^2. A scratch (1 mm × 35

μm) was made through the coating without damaging the aluminum substrate surface. The interested area was put in a flowing artificial seawater environment for one hour and then immersed into 0.1 M NaCl aqueous solution. The analyzed sample area was scanned within ca. 5 min, and the scans were repeated every 15 min. The subsequent analysis of the SVET data was performed with the help of homemade software to provide information about the minimal and maximal current densities in dependence of time. In a typical EIS (Electrochemical Impedance Spectroscopy) experiment, the coated substrates (6 × 3 cm^2) were placed into home-made cells, whereby an area of 3 cm^2 of the sample was exposed to 1 M NaCl solution at room temperature for 100 days. A reference (saturated calomel) and a counter (platinum) electrode were immersed in the cell. The coating on the opposite side of each sample was removed and the metal substrate, functioning as the working electrode, was connected to the potentiostat (CompactStat, Ivium Technologies). The current response was detected in the frequency range 100 kHz to 0.01 Hz at a constant potential (1 V) and a sinusoidal voltage signal of 10 mV. Six frequencies were typically assessed per order of magnitude of frequency.

4. Formation of Nanovalves

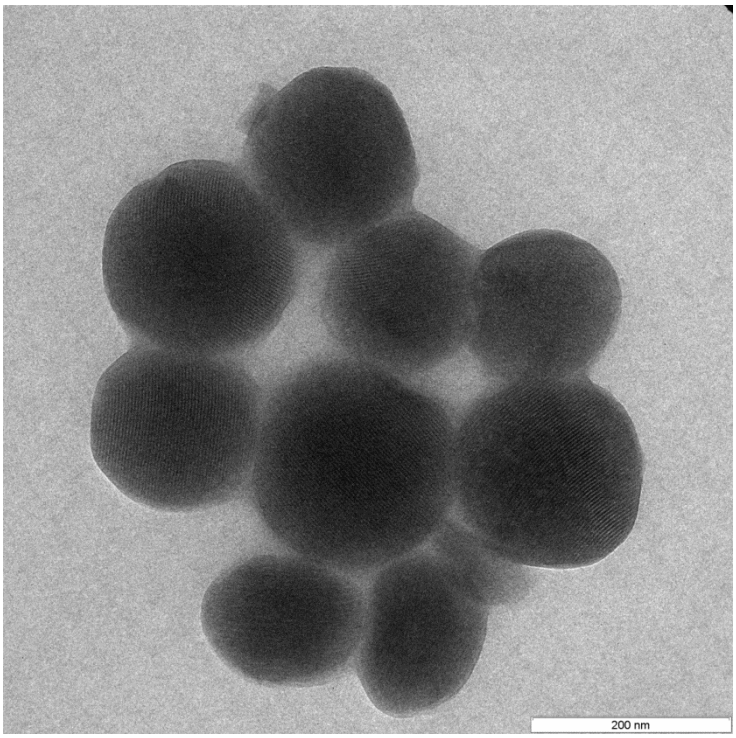

Fig. S1. TEM image of MCM-41 mesoporous silica nanoparticles functionalized with EDTA-type chelating agent.

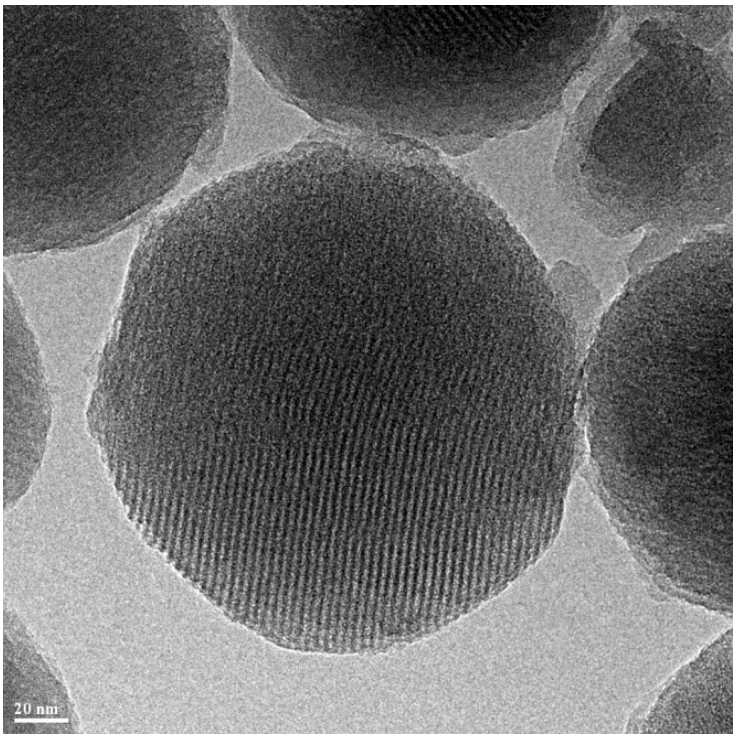

Fig. S2. TEM image of MCM-41 mesoporous silica nanoparticles with Co-Carbonate nanovalves.

The monodispersity and shape preservation of functionalized MCM-41 have been confirmed by TEM (Fig. S1). These particles maintain roughly pseudo-spherical shape and show negligible enlargement compared with native MCM-41, as their diameters are narrowly distributed in the range of 70-90 nm.

The TEM image (Fig. S2) of NPCs-inspired controlled release system reveals clearly that two-dimensional hexagonal p6mm ordered mesopores are also intact after the process of loading and formation of nanovalves.

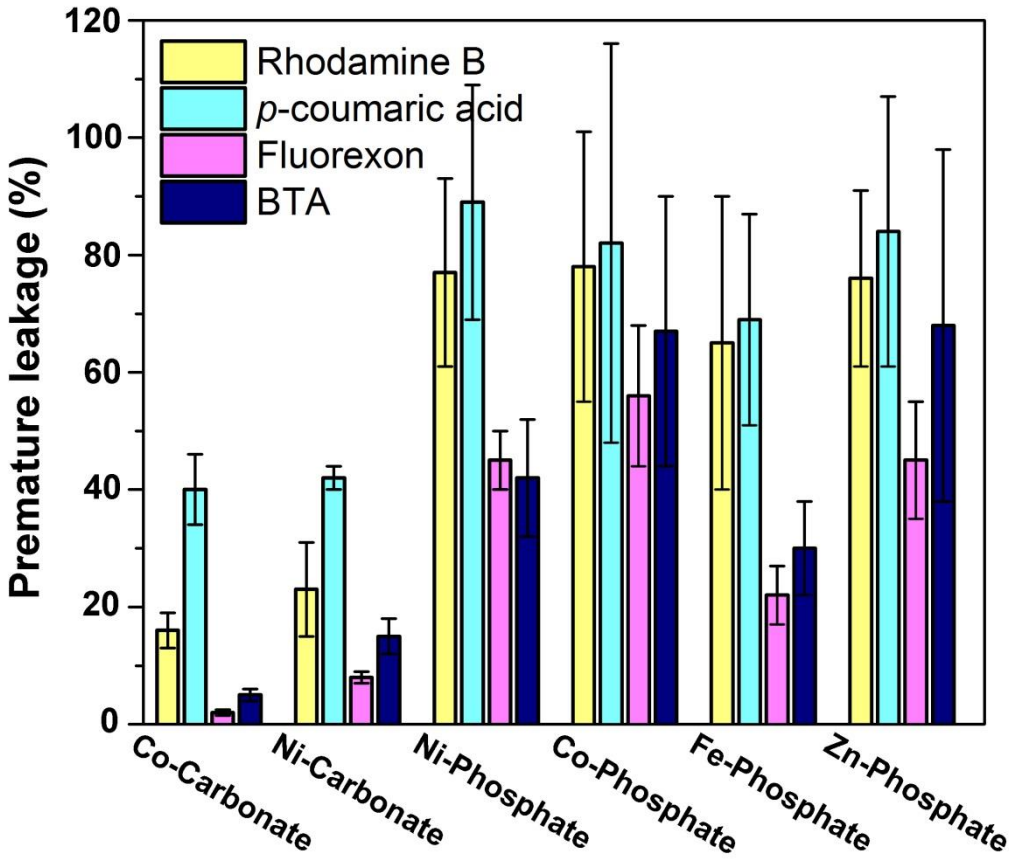

Fig. S3. The premature release (24 h) of different types of cargo from nanocontainers with different nanovalves.

1H-Benzotriazole ($C_6H_5N_3$, BTA) is widely used as a corrosion inhibitor for copper and other transition metals in many industries. It is a nitrogen heterocycle derivative containing three nitrogen atoms, each with an unshared lone pair of electrons, forming a five-membered ring that can exist in such tautomeric forms as following[3]:

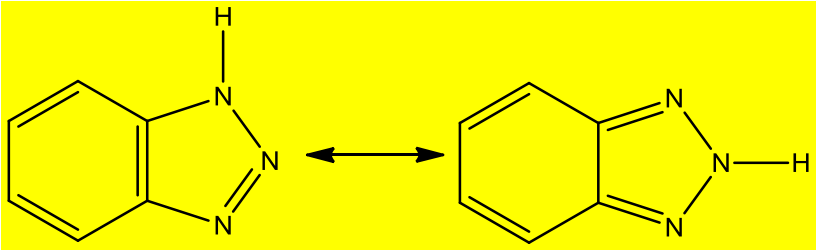

where the triazole ring plays a vital role in the formation of the complex with transition metal ions since the NH group, together with at least one other nitrogen atom, has been present before the complex will form.

5. Formation of Precipitates

For the process of forming precipitates, we injected 5 mL of $NaHCO_3$, $NaCO_3$, Na_3PO_4, Na_2HPO_4, NaH_2PO_4 and $(NaPO_3)_n$ solution quickly into the tube containing 5 mL of 0.1 M $NiCl_2$, $Co(NO_3)_2$, $Ca(NO_3)_2$, $CuSO_4$, $Mg(NO_3)_2$, $Zn(NO_3)_2$, $Fe(NO_3)_3$ and $Co(NH_3)_6Cl_3$ solutions to check whether the product was stable enough to achieve the notable precipitation. Most of the products are gelatinous precipitates (GP). After the formation of GPs, the previous salt solutions suddenly lose their fluidity and transparency. But with aging under atmospheric pressure and in room temperature, various changes can be observed, which are categorized as polymerization for increasing connectivity of the networks, coarsening resulting in expulsion of water, phase transformation due to reorganization of the structure and even oxidation of low valence metal ions. After aging for one day, we have focused on 6 types of GPs (a-f in **Table S1**) because they maintained the GP state without notable shrinkage in volume. Our record for the precipitates is summarized in **Table S1**.

Table S1. Library of products derived from rapid co-precipitation. I: keep GP state, II: condensed from GP without valence change, III: oxidized and condensed from GP, IV: clear

without precipitation and V: clear with bubbles during the whole day. Marked in the table is Ni-Carbonate (a), Ni-Phosphate (b), Co-Carbonate (c), Co-Phosphate (d), Zn-Phosphate (e) and Fe-Phosphate (f).

	$NaHCO_3$ 0.2 M	$NaCO_3$ 0.1 M	Na_3PO_4 0.1 M	Na_2HPO_4 0.1 M	NaH_2PO_4 0.2 M	$(NaPO_3)_n$ 0.2 M
$NiCl_2$ 0.1 M	1:1[a] **II**	2:1 **I**	5:1 **I**	2:1 **I**	1:1 **IV**	1:1 **IV**
	1:2 **II**	1:1 **I**	2:1 **I**	1:1 **I**	1:2 **IV**	1:2 **IV**
	1:4 **II**	1:2 **(a)** **I**	1:1**(b)** **I**	1:2 **I**	1:4 **IV**	1:4 **IV**

[a] molar ratio

$Co(NO_3)_2$ 0.1 M	1:1 **II**	2:1 **I**	5:1 **I**	2:1 **I**	1:1 **IV**	1:1 **IV**
	1:2 **II**	1:1 **I**	2:1 **I**	1:1 **I**	1:2 **IV**	1:2 **IV**
	1:4 **II**	1:2 **(c)** **I**	1:1**(d)** **I**	1:2 **I**	1:4 **IV**	1:4 **IV**
$Ca(NO_3)_2$ 0.1 M	1:1 **II**	2:1 **II**	5:1 **II**	2:1 **II**	1:1 **IV**	1:1 **II**
	1:2 **II**	1:1 **II**	2:1 **II**	1:1 **II**	1:2 **IV**	1:2 **II**
	1:4 **II**	1:2 **II**	1:1 **II**	1:2 **II**	1:4 **IV**	1:4 **II**
$CuSO_4$ 0.1 M	1:1 **II**	2:1 **II**	5:1 **I**	2:1 **II**	1:1 **II**	1:1 **IV**

	1:2 **II**	1:1 **I**	2:1 **I**	1:1 **II**	1:2 **II**	1:2 **IV**
	1:4 **II**	1:2 **I**	1:1 **I**	1:2 **II**	1:4 **II**	1:4 **IV**
$Mg(NO_3)_2$ 0.1 M	1:1 **IV**	2:1 **I**	5:1 **I**	2:1 **I**	1:1 **IV**	1:1 **I**
	1:2 **IV**	1:1 **I**	2:1 **I**	1:1 **I**	1:2 **IV**	1:2 **IV**
	1:4 **IV**	1:2 **I**	1:1 **I**	1:2 **I**	1:4 **IV**	1:4 **IV**
$Zn(NO_3)_2$ 0.1 M	1:1 **IV**	2:1 **I**	5:1 **I**	2:1 **I**	1:1 **IV**	1:1 **IV**
	1:2 **IV**	1:1 **I**	2:1 **I**	1:1 **(e)** **I**	1:2 **IV**	1:2 **IV**
	1:4 **IV**	1:2 **I**	1:1 **I**	1:2 **I**	1:4 **IV**	1:4 **IV**

	$NaHCO_3$ 0.2 M	$NaCO_3$ 0.1 M	Na_3PO_4 0.1 M	Na_2HPO_4 0.1 M	NaH_2PO_4 0.3 M	$(NaPO_3)_n$ 0.3 M
$Fe(NO_3)_3$ 0.1 M	1:1 **IV**	2:1 **V**	2:1 **I**	2:1 **I**	2:3 **I**	2:3 **I**
	1:2 **IV**	1:1 **V**	1:1 **(f)** **I**	1:1 **I**	1:3 **I**	1:3 **II**
	1:4 **IV**	1:2 **I**	1:2 **II**	1:2 **I**		

$Co(NH_3)_6Cl_3$ 0.1 M	1:1 **IV**	2:1 **IV**	2:1 **II**	2:1 **IV**	1:2 **IV**	1:2 **II**
	1:2 **IV**	1:1 **IV**	1:1 **II**	1:1 **IV**	1:4 **IV**	1:4 **II**
	1:4 **IV**	1:2 **IV**	1:2 **II**	1:2 **IV**		

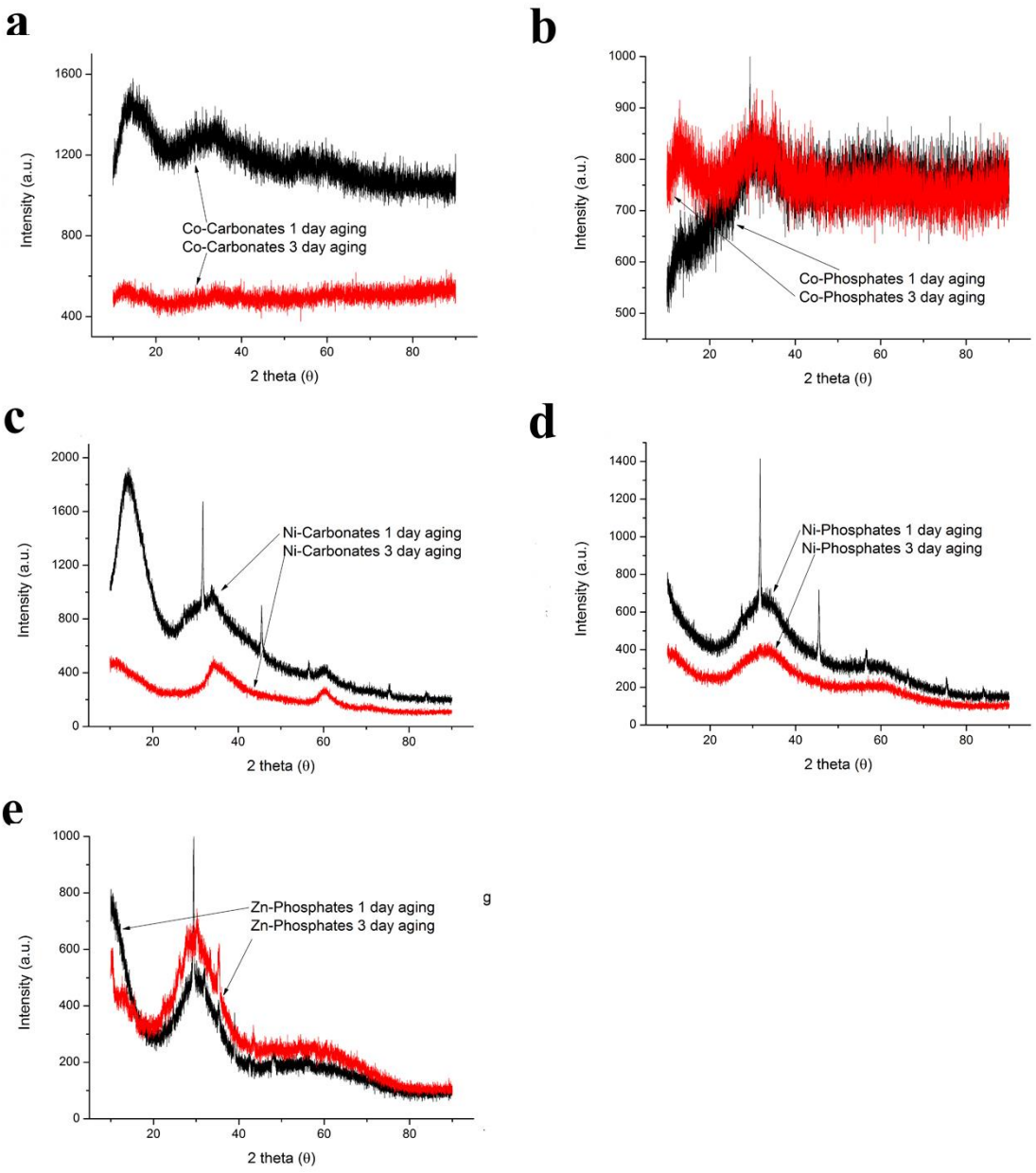

Fig. S4. XRD spectra of (a) Co-Carbonate, (b) Co-Phosphate, (c) Ni-Carbonate, (d) Ni-Phosphate and (e) Zn-Phosphate precipitates (marked as in Table S1) after one- and three-day aging. All the precipitates in our work maintained amorphous phase after aging for one day. After aging for three days, most of related precipitates maintained amorphous state.

The power law information derived from the Porod region of scattering for precipitates reveals fractal behavior. In the Porod region the scattered intensity decays as a power law: I (K) ~ K^{-D}. Fractal dimension, D = -2df + ds where D is obtained from the value of the slope at the Porod region, df is the mass fractal dimension ($0 \leq df \leq 3$) and ds is the surface fractal dimension ($2 \leq ds \leq 3$). The Guinier radius of the initial curvature of the SAXS curve can be obtained by the position of crossover, which is about K = 0.047 $Å^{-1}$. Thus the radius equals roughly 21 Å.

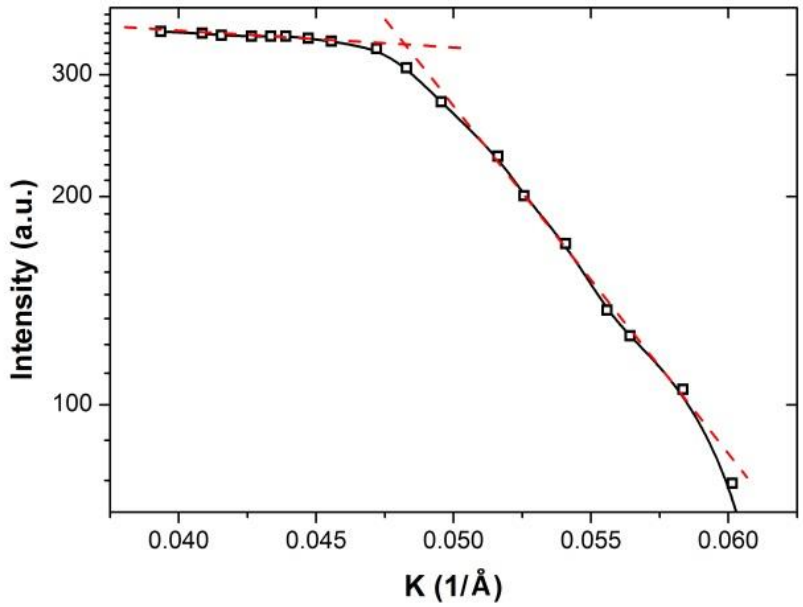

Fig. S5. Guinier regime of SAXS spectra of cobalt basic carbonate precipitates. The Guinier radius of the initial curvature of the SAXS curve can be simply obtained by the position of crossover.

Table S2. Relevant structural information about the selected precipitates.

Samples	S_{BET} (m^2g^{-1})		Pore volume (m^3g^{-1})		zeta (ξ) potentials (mV)
	1-day aging	3-days aging	1-day aging	3-days aging	
Ni-Carbonate	46.22	36.97	0.33	0.31	8.0 ± 0.2
Ni-Phosphate	52.28	42.55	0.44	0.39	-12.2 ± 0.2
Co-Carbonate	82.75	75.28	0.39	0.22	21.6 ± 0.9
Co-Phosphate	33.40	32.38	0.29	0.22	-18.2 ± 0.5
Fe-Phosphate	34.28	33.97	0.35	0.37	-38.7 ± 3.6
Zn-Phosphate	37.74	37.61	0.38	0.44	-47.3 ± 2.3

6. Diffusion test

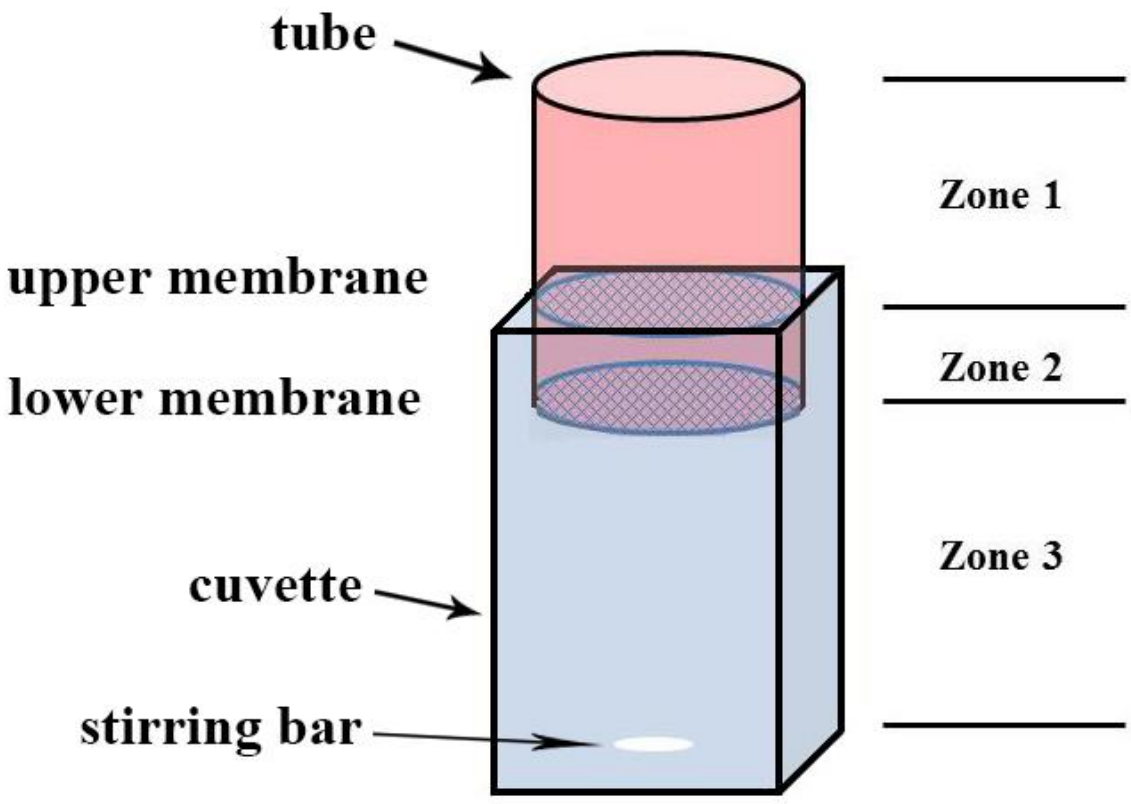

Scheme S1. Setup built for semi-quantitatively evaluation of precipitates.

To test permeability of the precipitates formed in our work, a modified cuvette utilized in fluorescence measurement was designed, as shown in Scheme S1. The precipitates or water were confined in a space, namely Zone 2, formed by upper membrane, lower membrane and inner wall of the tube that was inserted into cuvette with depth at 1 cm. Into Zone 1, 1 mL of starting solution was stored. A 5-mm stirring bar was added to the cuvette. The solution in Zone 3 was stirred moderately to balance the concentration of interesting molecules. The solution was monitored using a CCD detector which collected the emission spectra. A laser probe beam directed into the solution at 2 cm above the bottom and around 1 cm below the

top of the cuvette. Thus we can estimate the permeability of precipitates or water between two membranes by detecting fluorescence intensity of solution in the cuvette.

Modelling.

One layer diffusion. The modelling was based on semipermeable membrane diffusion study. The steady-state flux of solute through a semipermeable membrane (J) can be written as[4]:

$$J = \frac{dq}{a \cdot dt} = \frac{D_m}{H_m}(c_1 - c_2) \tag{3}$$

thus

$$c_2(t) = -c_1 \cdot e^{-At} + c_1 = c_1(1 - e^{-At}) \tag{4}$$

Where a is area of the membrane, H_m and H_1 are respectively heights of the membrane and the zone above upper membrane, c_1 and c_2 are the free solute concentrations at each interface $A = D_m / H_1 \cdot H_m$
of the membrane and D_{m} is the diffusion coefficient of the solute through the membrane. Let

.

Two layers diffusion: I. *Free diffusion*

On the basis of one layer diffusion study, we suppose concentration in the cuvette is:

$$c(t) = c_{t\to\infty}(1 - e^{-At}) \cdot erfc\left(\frac{F}{\sqrt{t}}\right) \cdot (1 - e^{-Bt}) \tag{1}$$

In eq. (1), $erfc\left(\frac{F}{\sqrt{t}}\right)$ is an error function, expressed as:

$$erfc(x) = 1 - erf(x) = \frac{2}{\sqrt{t}} \int_x^\infty e^{-t^2} dt \tag{5}$$

The parameter F here has an expression as $\frac{x}{2\sqrt{D}}$, where x is diffusion distance of solute from upper membrane and D is diffusion coefficient of solute between two membranes. The values of parameters A and B are determined by the fit of equation (1) when precipitates are replaced by water and then preset constantly prior to each fitting process.

Two layers diffusion: II. *Selective detaining*

The absorption of BTA onto metal surface generally obeys the Langmuir adsorption isotherm, which is

$$\theta = \frac{c \cdot L}{1 + c \cdot L}, \tag{6}$$

where θ is the fractional coverage of the surface, c is the concentration, L is Langmuir adsorption constant depicting the capacity of surface to absorb the solute. Then, the fraction of non-absorbed solute by precipitates is 1-θ. Thus, the concentration in cuvette is:

$$c(t) = c_{t\to\infty}(1 - e^{-At}) \cdot \left(\frac{1}{1 + c_{t\to\infty}(1 - e^{-At})L} \right) \cdot (1 - e^{-Bt}) \tag{2}$$

We utilize the software MATHEMATICA 7.0 to fit the responding experimental data by using the equations (1) and (2), respectively. The comparison of modeling and experimental results is shown in Figs. 3 (b) and (c).

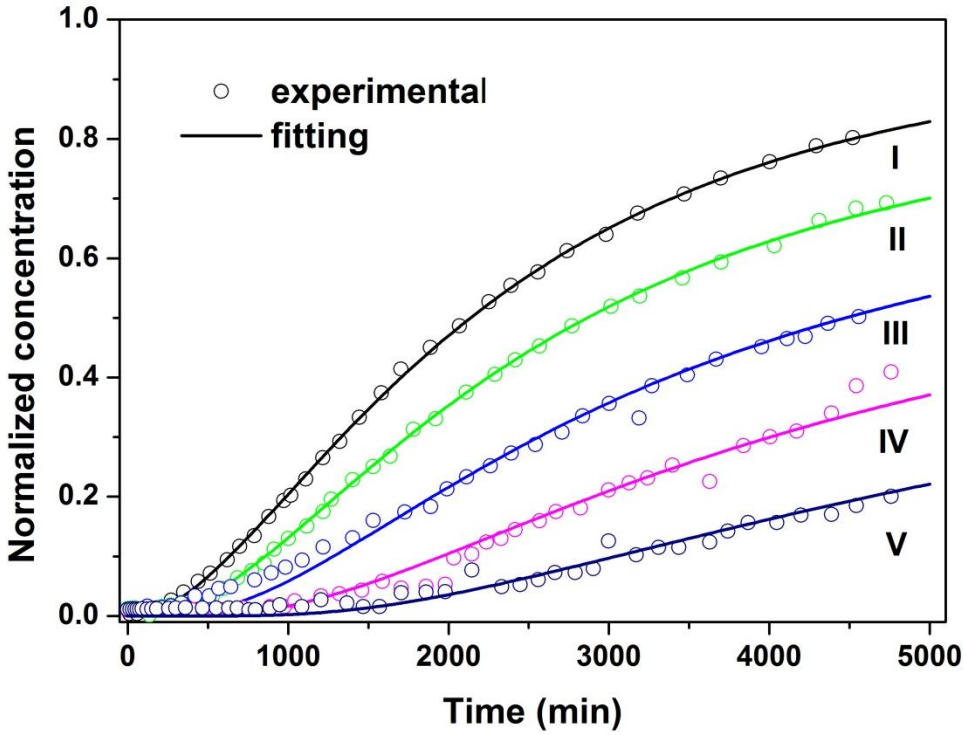

Fig. S6. The concentration of rhodamine B in cuvette (circle) as a function of time. All the data belonging to different samples have been normalized by the final equilibrium concentration in the case that the precipitates are replaced by water. The data in this study is reliable because the starting and ending concentrations of solutes fall into the linear range between fluorescence intensity and concentration. The theoretic fitting (solid curves) is consistent with the trend of experimental data of water (I, black), Co-Phosphate (II, Green), Ni-Phosphate (III, Blue), Co-Carbonate (IV, Magenta) and Ni-Carbonate (V, Navy).

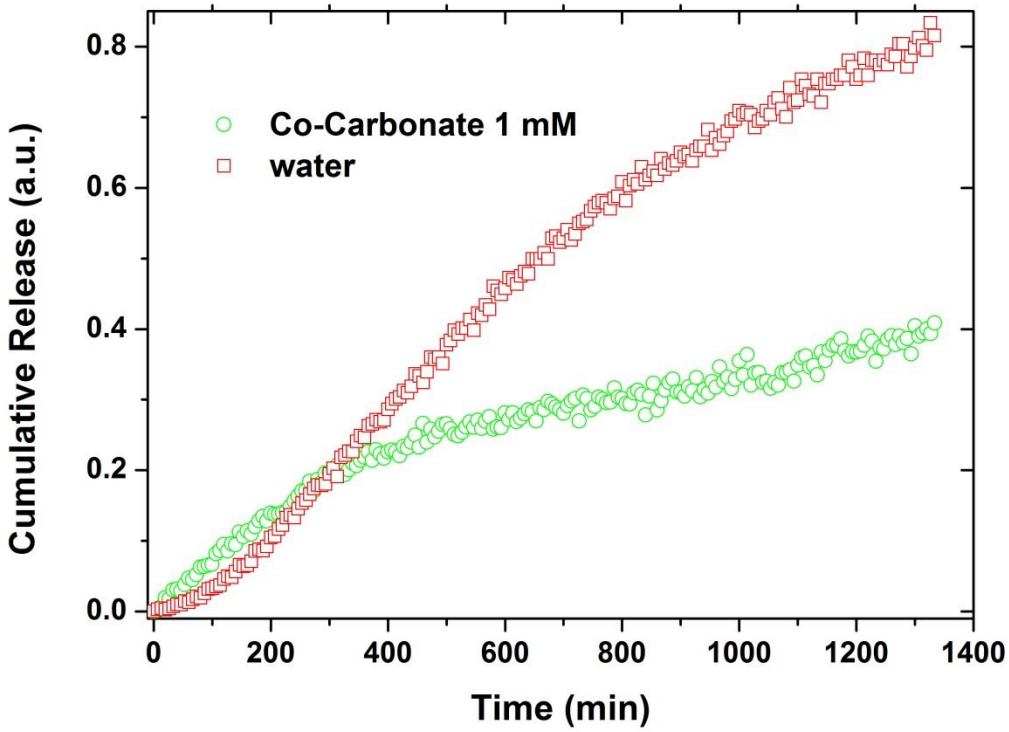

Fig. S7. The concentration of BTA in Zone III (circle) as a function of time as Zone II is filled by 1 mM (Green circle) Co-Carbonate precipitates and pure water with the concentration of starting solution 10 mg/L.

Water (red squares in Fig. S7) in Zone II allows BTA to freely diffuse, resulting in a good fit of equation (1), while 1 mM (Green) Co-Carbonate precipitates can detain 60% of BTA.

7. Anticorrosion test

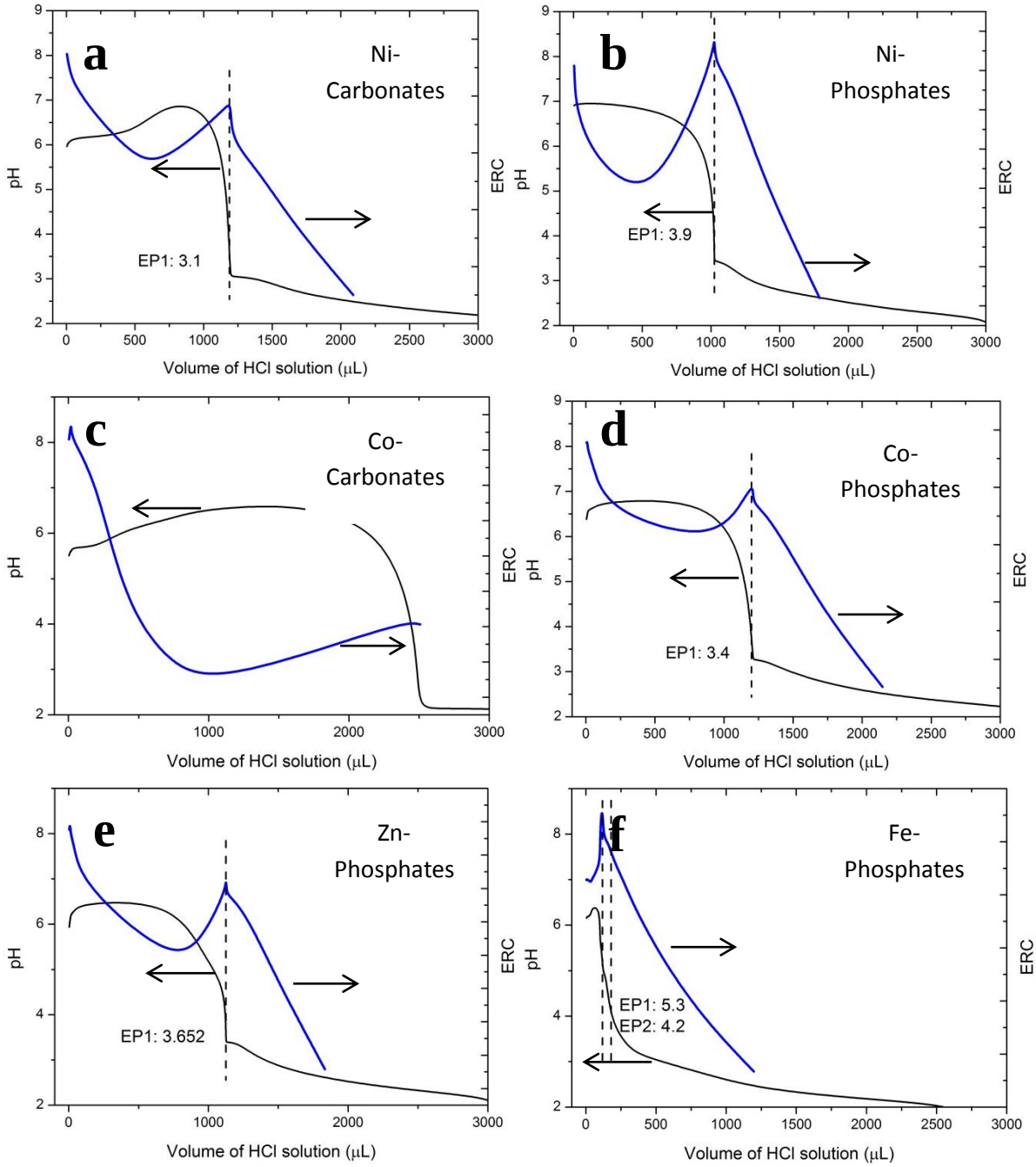

Fig. S8. Titration and exothermic profiles of some transition metal precipitates (marked in Table S1) and their exothermic points.

Possible reaction in the process of forming nanovalves and their response to pH lowering.

$[Co(H_2O)_6]^{2+}$ (*aq*) + CO_3^{2-} (*aq*) + OH^- (*aq*) → x $CoCO_3$ (*GP*) + (1-x) $Co(OH)_2$ (*GP*) + H_2O (1)

$CoCO_3$ (*GP*) + H^+ (*aq*) → $Co(HCO_3)_2$ (*s*)

$Co(HCO_3)_2$ (*s*) + H^+ (*aq*) + H_2O → $[Co(H_2O)_6]^{2+}$ (*aq*) + CO_2 + H_2O (2)

$Co(OH)_2$ (*GP*) + H^+ (*aq*) + H_2O → $[Co(H_2O)_6]^{2+}$ (*aq*) + H_2O (3)

8. References

1. S. Angelos, *et al.*. *Journal of the American Chemical Society* 2009, **131**, 12912-12913.
2. Z. Zheng, *et al. Advanced Functional Materials* 2013, **23**, 3307-3314.
3. C. Sease , *Stud. Conserv.* 1978, **23**, 76 – 85.
4. G.E. Amidon, W.I. Higuchi, NFH. Ho *J Pharm Sci* 1982, **71**, 77-84.